


RESEARCH

Open Access



Immune response and pathogen invasion at the choroid plexus in the onset of cerebral toxoplasmosis

Caio Andreeta Figueiredo¹, Johannes Steffen¹, Lorena Morton¹, Sushmitha Arumugam¹, Oliver Liesenfeld², Mária A. Deli³, Andrea Kröger⁴, Thomas Schüler⁵ and Ildiko Rita Dunay^{1,6*} 

Abstract

Background: *Toxoplasma gondii* (*T. gondii*) is a highly successful parasite being able to cross all biological barriers of the body, finally reaching the central nervous system (CNS). Previous studies have highlighted the critical involvement of the blood–brain barrier (BBB) during *T. gondii* invasion and development of subsequent neuroinflammation. Still, the potential contribution of the choroid plexus (CP), the main structure forming the blood–cerebrospinal fluid (CSF) barrier (BCSFB) have not been addressed.

Methods: To investigate *T. gondii* invasion at the onset of neuroinflammation, the CP and brain microvessels (BMV) were isolated and analyzed for parasite burden. Additionally, immuno-stained brain sections and three-dimensional whole mount preparations were evaluated for parasite localization and morphological alterations. Activation of choroidal and brain endothelial cells were characterized by flow cytometry. To evaluate the impact of early immune responses on CP and BMV, expression levels of inflammatory mediators, tight junctions (TJ) and matrix metalloproteinases (MMPs) were quantified. Additionally, FITC-dextran was applied to determine infection-related changes in BCSFB permeability. Finally, the response of primary CP epithelial cells to *T. gondii* parasites was tested in vitro.

Results: Here we revealed that endothelial cells in the CP are initially infected by *T. gondii*, and become activated prior to BBB endothelial cells indicated by MHCII upregulation. Additionally, CP elicited early local immune response with upregulation of IFN- γ , TNF, IL-6, host-defence factors as well as swift expression of CXCL9 chemokine, when compared to the BMV. Consequently, we uncovered distinct TJ disturbances of claudins, associated with upregulation of MMP-8 and MMP-13 expression in infected CP in vivo, which was confirmed by in vitro infection of primary CP epithelial cells. Notably, we detected early barrier damage and functional loss by increased BCSFB permeability to FITC-dextran in vivo, which was extended over the infection course.

Conclusions: Altogether, our data reveal a close interaction between *T. gondii* infection at the CP and the impairment of the BCSFB function indicating that infection-related neuroinflammation is initiated in the CP.

Keywords: *Toxoplasma gondii*, Neuroinflammation, Choroid plexus, Blood–CSF barrier, Blood–brain barrier, Tight junctions, Matrix metalloproteinases

Background

Toxoplasmosis is a foodborne parasitic disease caused by the obligate intracellular protozoan *Toxoplasma gondii* (*T. gondii*). It is estimated that more than one-third of the world's human population is infected with *T. gondii* and

*Correspondence: ildikodunay@gmail.com

¹ Institute of Inflammation and Neurodegeneration, Medical Faculty, Otto-Von-Guericke University Magdeburg, Magdeburg, Germany
Full list of author information is available at the end of the article



© The Author(s) 2022. **Open Access** This article is licensed under a Creative Commons Attribution 4.0 International License, which permits use, sharing, adaptation, distribution and reproduction in any medium or format, as long as you give appropriate credit to the original author(s) and the source, provide a link to the Creative Commons licence, and indicate if changes were made. The images or other third party material in this article are included in the article's Creative Commons licence, unless indicated otherwise in a credit line to the material. If material is not included in the article's Creative Commons licence and your intended use is not permitted by statutory regulation or exceeds the permitted use, you will need to obtain permission directly from the copyright holder. To view a copy of this licence, visit <http://creativecommons.org/licenses/by/4.0/>. The Creative Commons Public Domain Dedication waiver (<http://creativecommons.org/publicdomain/zero/1.0/>) applies to the data made available in this article, unless otherwise stated in a credit line to the data.

its seroprevalence increases gradually with age [1–3]. Following uptake via oral ingestion of contaminated food or water, the parasites proliferate within a variety of nucleated cells, infect circulating leukocytes, successfully cross all the barriers of the body and spread throughout host tissues [4]. Despite of the central nervous system (CNS) being an immune privileged site shielded from peripheral infections and inflammation, *T. gondii* parasites are able to invade the CNS. Previous studies have proposed different mechanisms of parasite invasion, including: (1) active paracellular migration of free parasites; (2) transmigration of hypermotile infected leukocytes, defined as “Trojan horse” mechanism, and (3) infection and replication of parasites within brain endothelial cells [5–12]. Once *T. gondii* crosses the brain biological barriers, like the blood–brain barrier (BBB), they invade brain-resident cells and persist in cysts lifelong [13–15]. The cyst formation within neurons develops a stress-mediated response followed by ongoing basal neuroinflammation, which leads to altered neuronal function, and potentially to behavioral alterations and neuropsychiatric diseases [16–19]. In immunodeficient individuals, the infection can lead to disruption of tissue cysts and uncontrolled parasite proliferation, resulting in toxoplasma encephalitis (TE) [2, 20, 21].

Several studies have demonstrated the decisive involvement of the BBB in the invasion of *T. gondii* and the ensuing development of neuroinflammation [22, 23]. In fact, the choroid plexus (CP) is another barrier and potential interface for pathogen invasion into CNS. The CP is the main structure forming the blood–CSF barrier (BCSFB), and is crucial for CNS homeostasis and cerebrospinal fluid (CSF) secretion. Located within the four brain ventricles, the CP is a villous and selective organ formed by adjacent epithelial cells anchored to a basal lamina and an inner core of resident immune cells surrounding a dense vascular network of fenestrated endothelial cells. Choroidal epithelial cells are tightly interconnected by tight junction proteins (TJ), and control the molecular and cellular composition of the CSF [24, 25]. The ability of this unique neuro-immune interface to actively integrate signals between brain and periphery is fundamental to CNS immunity [26], in which CP regulation of immune cell trafficking is considered a central point in the initiation of inflammatory brain responses [27]. Alterations or even disruption of the CP epithelium in response to stressful events have detrimental effects on barrier permeability compromising the BCSFB functions [28]. Indeed, BCSFB breakdown has been implicated in neurodegenerative diseases [29–33] and during infection-induced inflammation [31, 34], often indicating the involvement of matrix metalloproteinases (MMPs). Moreover, recent studies have described that the BCSFB serves as a hotspot for

direct pathogen infiltration into the CNS [35]. However, data concerning the contribution of the CP to *T. gondii* invasion, and subsequent neuroinflammation are controversial and incomplete. For example, the analysis of post-mortem samples from immunodeficient patients with cerebral toxoplasmosis identified the CP as a site of infection [36]. On the contrary, models of reactivated TE indicate no evidence for the involvement of CP in systemic parasitic dissemination [37, 38].

Here, we demonstrate that, prior to the activation of endothelial cells in the BBB, parasites invading the CNS rapidly seize choroidal endothelial cells. As a result, a prompt immune response is initiated in the CP as shown by the upregulation of cytokines, chemokines, and host defense factors, followed by the expression of MMPs, TJ disturbance of CP epithelial cells, and subsequent increased barrier permeability. Together, our results show that the infection takes place in the CP, and indicate sudden functional impairment of the BCSFB upon the onset of the CNS invasion by *T. gondii*.

Methods

Mice and infections in vivo

Experiments were conducted with female C57BL/6 J mice (8–14 weeks old, purchased from Janvier, Cedex, France). All animals were group-housed in a 12-h day/night cycle at 22 °C with free access to food and water under specific pathogen-free conditions and according to institutional guidelines approved by the Animal Studies Committee of Saxony-Anhalt. In order to investigate early *T. gondii* infection, mice were infected by intraperitoneal (*i.p.*) injection of either cysts or tachyzoites. For cyst infection, 2 cysts of the type II ME49 strain harvested from the brains of female NMRI mice infected *i.p.* with *T. gondii* cysts 6–12 months earlier were used as previously described [39]. For tachyzoites infection, type II *T. gondii* reporter parasites of the PTG-GFPS65T strain were grown in monolayers of human foreskin fibroblast (HFF) with DMEM medium (FG0435, Biochrom, Germany), supplemented with 10% fetal bovine serum (FBS) (ThermoFisher, Germany), 1% penicillin/streptomycin (Pen/Strep; Sigma, USA) and 1% non-essential amino acids (NEEA) (ThermoFisher, Germany) as previously described [40]. Freshly egressed parasites were filtered through a 5 µm Millex-SV syringe filter (Millipore, Germany), and the number of living tachyzoites determined by counting under a bright-field microscope using Trypan Blue 0.4%. Mice were infected *i.p.* with 1×10^5 reporter parasites in 200 µl PBS.

Organ isolation

Mice were deeply anaesthetized by isoflurane inhalation (Baxter), the CSF was collected and thereafter animals

were transcardially perfused with 60 ml PBS. For immunofluorescence samples, perfusion was additionally done with 20 ml of 4% paraformaldehyde (PFA) in PBS. Brain, spleen and spinal cord were removed and stored in sterile ice-cold PBS or RNAlater (Sigma) for further processing. Samples stored in RNAlater were kept at 4 °C overnight and afterwards transferred to - 80 °C.

Cerebrospinal fluid collection

CSF was collected by the *cisterna magna* puncture technique as described elsewhere [41]. In short, deeply anaesthetized animals were immobilized in a prone position with the head forming a 135° angle with the body, and a sagittal incision of the skin was made inferior to the occiput. Using a stereomicroscope (Stemi 305; ZEISS), the subcutaneous tissue and muscles were dissected, and a glass capillary tube was introduced into the *cisterna magna* through the dura matter, lateral to the *arteria dorsalis spinalis*. An average of 15 µl of CSF per animal were collected, and kept on ice until further processing. Samples were macroscopically assessed for blood contamination, and discarded when contamination was detected.

Choroid plexus and brain tissue isolation

Isolated brains were placed under a stereomicroscope in dissection buffer containing HBSS (ROTI®Cell, Roth), and 10 mM HEPES (Gibco, ThermoFisher). CPs were isolated from the lateral, third and fourth brain ventricles, and were either processed for total RNA/DNA isolation, or placed in digestion buffer for further cell isolation. Cerebellum, olfactory bulbs, and adjacent brain meninges were removed and discarded. The remaining brain tissue was used for cell isolation followed by flow cytometric analysis, or further utilized for brain microvessels isolation.

Brain microvessels isolation

Brain microvessels were isolated as previously described [42] with a few modifications, and used for immunofluorescence, or total RNA/DNA isolation. Briefly, brain hemispheres were minced with a scalpel, and homogenized in digestion buffer (HBSS, with 6.75 g/l glucose, 20 mM HEPES) containing 1 mg/ml DNase I. After incubation (10 min, 37 °C), homogenate was washed in FACS buffer (PBS w/o Ca/Mg, 2 mM EDTA, 2% v/v FBS, 10 mM HEPES). The resultant pellet was resuspended and separated by successive centrifugations in 20% (w/v) bovine serum albumin (BSA)-DMEM/F12 solution. To remove remaining myelin debris, the pellet containing microvessels was resuspended in PBS, fractionated on 22% (v/v) Percoll® (Sigma, #GE17089101) gradient solution and centrifuged for 10 min, 600 × g, w/o brake. The

microvessels pellet was recovered and extensively washed in PBS/HEPES.

Cell isolation

Isolated CP, the remaining brain tissue, liver and lymph nodes (inguinal and mesenteric) were further processed in order to obtain single cell suspensions. CP samples were incubated (20 min, 37 °C) in digestion buffer (PBS w/ Ca/Mg, 2% v/v FBS, 10 mM HEPES) containing 1 mg/ml DNase I (Sigma, #DN25) and 1 mg/ml Collagenase/Dispase (Sigma, #11097113001). Digested tissues were mechanically dissociated using syringes connected to 22- and 26G needles, then cells were washed with FACS buffer, and used for further analysis. For the isolation of brain cells, liver and lymph nodes, tissues were minced with a scalpel, and homogenized in digestion buffer (HBSS, with 6.75 g/l glucose, 20 mM HEPES) containing DNase I and Collagenase/Dispase as previously mentioned. Homogenate was incubated (40 min, 37 °C, 200 rpm), and filtered through a 70-µm cell strainer (Falcon®, #352350). The cell suspension was centrifuged (400 × g, 10 min, 4 °C), and the cell pellet separated in a 25–70% discontinuous Percoll® gradient for 20 min without brake. Cells were recovered from the gradient interface, washed with FACS buffer, and used for further analysis.

Flow-cytometric analysis

Cells were resuspended in FACS buffer, and stained as previously described [39, 40]. In short, cells were incubated with an anti-mouse CD16/32 unconjugated antibody (clone 93, BioLegend) and stained with fixable viability dye Zombie NIR (BioLegend), for 20 min at 4 °C. Subsequently, cells were stained (30 min, 4 °C) using fluorochrome-conjugated antibodies. CD11b (PerCP-Cy5.5, clone M1/70) purchased from eBioscience, CD45 (BV510, clone 30-F11), MHCII (BV711, clone M5/114.15.2), VE-cadherin (BV421, clone BV13), and gp38 (AF488, clone PMab-1) purchased from BioLegend. CD31 (APC, clone MEC13.3) purchased from BD Biosciences. Cells were washed (400 × g, 5 min 4 °C) with FACS buffer, fixed in 4% PFA for 15 min at 4 °C and re-suspended in FACS buffer. For CP, cells were additionally permeabilized with eBioscience™ Permeabilization buffer (Invitrogen), incubated with antibody rabbit-anti-TTR (Abcam) for 40 min, and stained with secondary antibody anti-rabbit AF488 (ThermoFisher). Cells were acquired using Attune NxT Flow Cytometer (ThermoFisher). Data were analyzed using FlowJo software (version 10.5.3, FlowJo LLC, OR, USA).

FITC-dextran permeability assay

BCSFB and BBB permeability were measured as previously described [34] with modifications. In short, 4 kDa FITC-dextran (Sigma, #46944) was diluted in PBS, and administered intravenously (*i.v.*) at 75 mg/kg body weight mice, 30 min before CSF and brain collection. CSF was collected through the *cisterna magna* as previously described, diluted 100-fold in PBS, and spun down (1000 × g, 5 min). The resulting supernatant was further used for analysis. After perfusion, isolated brains were weighted, minced with a scalpel, homogenized in formamide (Roth) at 0.8 ml per 100 mg tissue, and incubated overnight (37 °C, 200 rpm). Homogenates were spun down (12,000 × g, 5 min), and supernatants were collected and diluted twofold in PBS. All samples were measured in triplicates at $\lambda_{ex}/\lambda_{em}=485/520$ nm using SpectraMax M5e (Molecular Devices LLC).

Choroid plexus epithelial cells and *T. gondii* in vitro infection

Primary CP epithelial cell culture was obtained as previously described [43, 44] with modification. Isolated CP from 9 to 14 mice, one-week-old, were used in each preparation. Tissues were pooled in digestion buffer (PBS w/ Ca/Mg, 2% v/v FBS, 10 mM HEPES) containing 1 mg/ml DNase I and 2 mg/ml Collagenase/Dispase, and incubated (20 min, 37 °C). Digested tissues were mechanically dissociated and cells were washed (400 × g 5 min) with FACS buffer (PBS w/o Ca/Mg, 2 mM EDTA, 2% v/v FBS, 10 mM HEPES). Cell pellet was resuspended, and cultivated with complete medium (DMEM/F12, supplemented with 10% FBS, 1% penicillin/streptomycin, 1% ITS (insulin–transferrin–selenite), 40 mg/ml human-EGF (epidermal growth factor, PeproTech, Germany, #AF-100–15). Cells were grown until confluence, for approximately 7 to 10 days, in 12 well plates previously coated with poly-L-lysine (PLL), or on top of PLL-coated coverslips. Once confluent, cells were infected at multiplicity of infection (MOI)=5 with type II PTG-GFPS65T tachyzoites, and incubated at 37 °C. After 6 h, culture medium was removed, cells were washed with PBS, and further used for total RNA/DNA isolation, flow cytometric analysis (validation) or immunofluorescence. Naïve controls were treated with pre-warmed fresh medium.

Immunofluorescence

Immunofluorescence staining was performed for CP whole mount, BMV mount, brain sections and cell culture coverslips. For brain sections, isolated brains were post-fixed (4 h, at 4 °C), soaked in 30% sucrose in PBS (2 days, at 4 °C), and frozen in cryo media (OCT Compound, Tissue Tek). Coronal sections (20 µm) were obtained (Thermo Scientific CryoStar NX50) and only

sections containing CP were stained. BMV mount, brain sections and coverslips were stained directly on glass slides. CP whole mount staining were performed utilizing a free-floating approach. All samples from different origins were stained and mounted with the same protocol unless otherwise stated. In short, samples were fixed (4% PFA in PBS, 20 min, 4 °C), washed twice with washing solution (PBS 0.1% (v/v) Triton X-100), and blocked/permeabilized with PBS 0.3% (v/v) Triton X-100 5% normal-goat-serum (NGS) and unconjugated F(ab')₂-goat anti-mouse IgG (H+L) antibody (1:500, Thermo Scientific), for 2 h at 4 °C. Next, samples were incubated with antibody solution (PBS 0.1% (v/v) Triton X-100 2% NGS) containing the primary antibodies of interest: anti-SAG1 (1:50, clone D61S, ThermoFisher), anti-GFP (1:1000, #132004, SYSY), anti-E-cadherin (1:500, #PA5-85088, ThermoFisher), anti-PDGFRβ (1:200, clone R.140.4, ThermoFisher), anti-ZO-1(1:50, clone R26.4C, ThermoFisher), anti-IBA-1(1:500, #234004, SYSY), anti-CD31 (1:50, clone MEC13.3, BioLegend), anti-claudin-2 (1:500, clone MH44, ThermoFisher), VE-cadherin (1:40, clone BV13, ThermoFisher). Primary antibodies were incubated overnight at 4 °C, then samples were washed twice, and incubated (30 min, RT) in antibody solution with secondary antibodies (1:1000) tagged with AF488, AF555, AF594 and AF647 according to each antibody host. Next, samples were washed twice, and mounted with ProLong™ Gold Antifade Mountant with DAPI (ThermoFisher). In some samples, anti-CD45 (clone 30-F11) conjugated antibody was used, and an additional final staining step was added. For brain sections, antigen retrieval (10 mM citrate buffer, pH 6.0, 0.1% Tween-20) was performed at 96 °C for 30 min, before the blocking and permeabilization step. Images were generated using a Leica TCS SP8 microscope, and analyzed using the ImageJ software (ImageJ 1.52p).

DNA and RNA isolation

Total DNA and RNA were isolated from CP, BMV, spleen, spinal cord, brain and CP epithelial cell culture. Samples from CP, BMV and CP epithelial cell culture were isolated with Quick-DNA/RNA Miniprep kit (Zymo Research, Germany) according to the manufacturer's instructions. Brain, spinal cord, and spleen samples were first homogenized with TriFast (Peqlab, 30-2010) using tubes containing Zirconium oxide beads (Precellys, P000926-LYSK0-A) in a BeadBug 6 homogenizer (Biozym). DNA was isolated from the homogenate according to the manufacturer's instructions. RNA was isolated from the homogenate by isopropanol precipitation or using peqGOLD total RNA kit (Peqlab) following the manufacturer's instructions. The concentration and purity of DNA and RNA samples were determined using

NanoDrop 2000 spectrophotometer (ThermoFisher; Germany), and samples were stored at -80°C until further use.

qPCR

Parasite burden was assessed in triplicates using 40 ng of isolated DNA, FastStart Essential DNA Green Master and LightCycler[®] 96 System (both Roche, Germany), as previously described [40]. Thermal-cycling parameters were set as follows: initial activation (95°C , 10 min), 55 amplification cycles consisting of denaturation (95°C , 15 s), annealing (60°C , 15 s) and elongation (72°C , 15 s). The DNA target was the published sequence of the highly conserved 35-fold-repetitive B1 gene of *T. gondii* [45, 46]. Murine argininosuccinate lyase (*Asl*) was used as reference gene for normalization and relative DNA levels were determined by the ratio *gene of interest/reference gene* and subsequently normalized to mean values of control group [47]. Primers were synthesized by Tib MolBiol (Germany) and used at 200 nM final concentration. Primer sequences are described elsewhere [see Additional file 1].

RT-qPCR

Gene expression levels of cytokines, inflammatory mediators, host-defense factors, tight junctions and MMPs were assessed in triplicates using 20 ng total RNA, TaqMan[®] RNA-to-CT[™] 1-Step Kit (Applied Biosystems, Germany) and LightCycler[®] 96 (Roche, Germany) as previously described [40]. Thermal-cycling parameters were set as follows: reverse transcription (48°C , 30 min), inactivation (95°C , 10 min) followed by 55 cycles of denaturation (95°C , 15 s) and annealing/extension (60°C , 1 min). Utilized TaqMan[®] Gene Expression Assays (Applied Biosystems, Germany) are listed elsewhere [see Additional file 1]. *Hprt* was chosen as *reference gene* and relative mRNA levels were determined by the ratio *gene of interest/reference gene* and subsequently normalized to mean values of control group.

For the genes analyzed using SYBR Green technology, Power SYBR[®] Green RNA-to-CT[™] 1-Step Kit (Applied Biosystems, Germany) was used. Samples were analyzed in triplicates (20 ng of isolated mRNA per reaction) using LightCycler[®] 96 with the following parameters: reverse transcription (48°C , 30 min), inactivation (95°C , 10 min) followed by 55 cycles of denaturation (95°C , 15 s) and annealing/extension (60°C , 1 min) and melting curve analysis. The primer sequences are listed elsewhere [see Additional file 1] and were synthesized by Tib MolBiol and used at 100 nM final concentration. *Hprt* was chosen as reference gene and relative mRNA levels were determined by the ratio *gene of interest/reference gene* and subsequently normalized to mean values of control group.

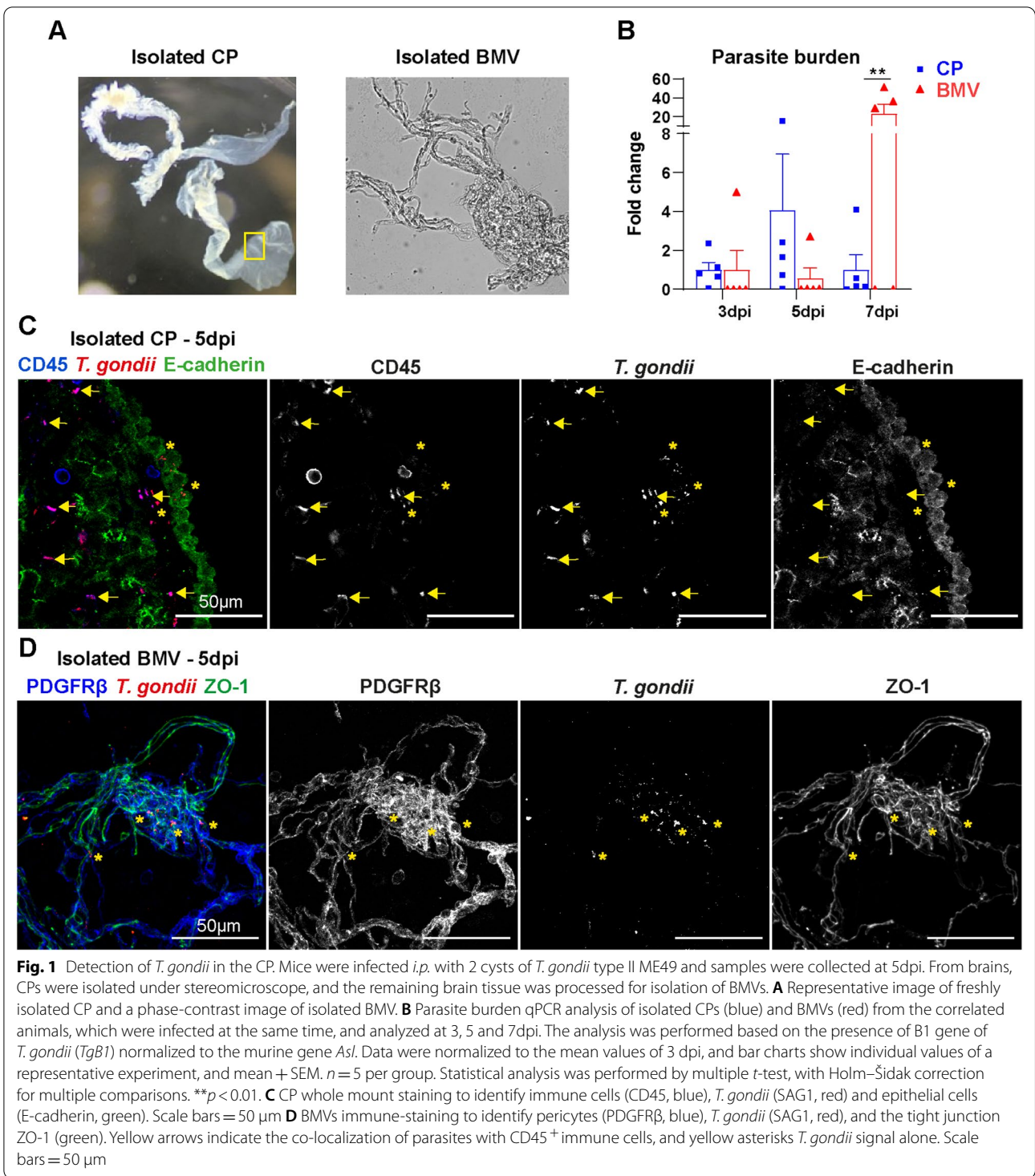
Statistical analysis

Results were statistically analyzed using GraphPad Prism 7 (GraphPad Software Inc., USA), *post-test* corrections were applied according to software recommendations. Statistical significance was set to $p \leq 0.05$. All data are presented as arithmetic mean and standard error of the mean (SEM) and are representative of at least two independent experiments. For parasite burden analysis, normalized data were analyzed by multiple *t*-test, with Holm–Šidák correction for multiple comparisons. For flow cytometric analyses, normalized data were analyzed by one-way ANOVA, with Tukey's correction. For RT-qPCR, data were analyzed by one-way ANOVA followed by Dunnett's correction. BCSFB permeability assay was analyzed by multiple *t*-test to compare between BCSFB and BBB, and one-way ANOVA followed by Dunnett's correction was used to compare differences between day 0 and the time-point analyzed from the same barrier type. RT-qPCR data from primary cell culture were analyzed by Student's *t*-test.

Results

Choroid plexus is infected by *T. gondii* upon the invasion

BCSFB is a gateway to the CNS for different pathogens as well as immune cells under certain inflammatory conditions [26, 35, 48–50]. Assuming that the CP is involved in the parasite entry and early immune response upon the invasion of the brain by *T. gondii*, we investigated the presence of parasites in the CNS through the course of infection. As BBB endothelial cells were shown previously to be directly infected by *T. gondii* [7], we isolated brain microvessels (BMV) that contain endothelial cells, and compared them to isolated CP (Fig. 1A) for parasite burden over time by PCR. Our results revealed the early presence of parasites on CP at 3 dpi, which was increased by day 5 and reduced by day 7 (Fig. 1B). In the BMV, the parasite burden only strongly increased by day 7 (Fig. 1B). Next, CP and BMV of infected animals were isolated and immuno-stained as a three-dimensional whole mount preparation. Within the CP at 5 dpi, we detected parasites (SAG1^+) co-localized with immune cells (CD45^+) (Pearson's coefficient, $r=0.57$), and also extracellular parasites present in the paracellular and stromal regions between the CP epithelial cells (E-cadherin^+) without co-localization with E-cadherin (Pearson's coefficient, $r=0.013$) (Fig. 1C). In the BMV, parasites were found to be associated to the microvasculature, although no co-localization were detected for $\text{PDGFR}\beta^+$ pericytes (Pearson's coefficient, $r=0.099$) and only a few for ZO-1^+ endothelial cells (Pearson's coefficient, $r=0.112$) (Fig. 1D), which constitute the main components of cerebral microvasculature forming the BBB [51]. Overall, parasites were found in the CP, and apparently more frequently in initial



infection at the BCSEFB interface than the BBB. Immunostaining of isolated BMV confirmed the presence of *T. gondii* tachyzoites in BMV at 7 dpi, as detected previously by PCR [see Additional file 2]. Splens were used as controls to monitor the parasite burden levels in the

periphery, indicating the usual spread of the parasites throughout tissues [see Additional file 2]. Parasite burden was just detected starting at 7 dpi in both brain parenchyma (after CP removal) and spinal cord, evidencing the

early infection through the CP and the microvasculature [see Additional file 2].

Choroid plexus endothelial and immune cells are targeted by *T. gondii*

Given the early presence of *T. gondii* in the CP, we sought to determine the target cell types in this compartment. Therefore, mice were infected *i.p.* with 10×10^5 tachyzoites of the *T. gondii* strain expressing the fluorescent protein GFP (PTG-GFPS65T). First, we analyzed coronal brain sections showing CP from lateral ventricles and found parasites within the choroidal endothelial cells at 7 dpi (Fig. 2A) [and see Additional file 3]. Indeed, at 7 dpi parasites were additionally found in the cortex and the adjacent brain areas [see Additional file 2], simultaneously to the CP [see Additional file 3]. To identify infected immune cells in the BCSFB, isolated CP whole mounts were co-stained for CD45 and CD31. At 3 dpi, we observed *T. gondii* parasites associated to immune cells and endothelial cells in the CP (Fig. 2B). Of note, recruited amoeboid-shape CD45^{hi} leukocytes did not appear to be associated to parasites, rather a resident stellate CD45^{int} CP macrophages (referred as CP-BAMs (border-associated-macrophages) or epiplexus cells) were co-localized with parasites at this time-point [see Additional file 3]. CP-resident macrophages were also identified by IBA-1 staining and morphology [see Additional file 4]. CP endothelial cells were infected with intracellular parasites at 3 and 5 dpi, but at 7 dpi infected cells were less abundant. Additionally, parasites were also found in the inner core of the CP parenchyma, suggesting the infection of mesenchymal derived stromal cells. Altogether, our results demonstrate the dynamic infiltration of parasites into endothelial and immune cells of the CP in the early phase of infection, confirming our initial data on parasite burden.

Early immune response at the choroid plexus prior to the BBB

Pathogens infecting the CP elicit local immune responses which are associated with the activation of endothelial, epithelial and tissue-resident immune cells [35]. To characterize the early immune response to *T. gondii* in the CP

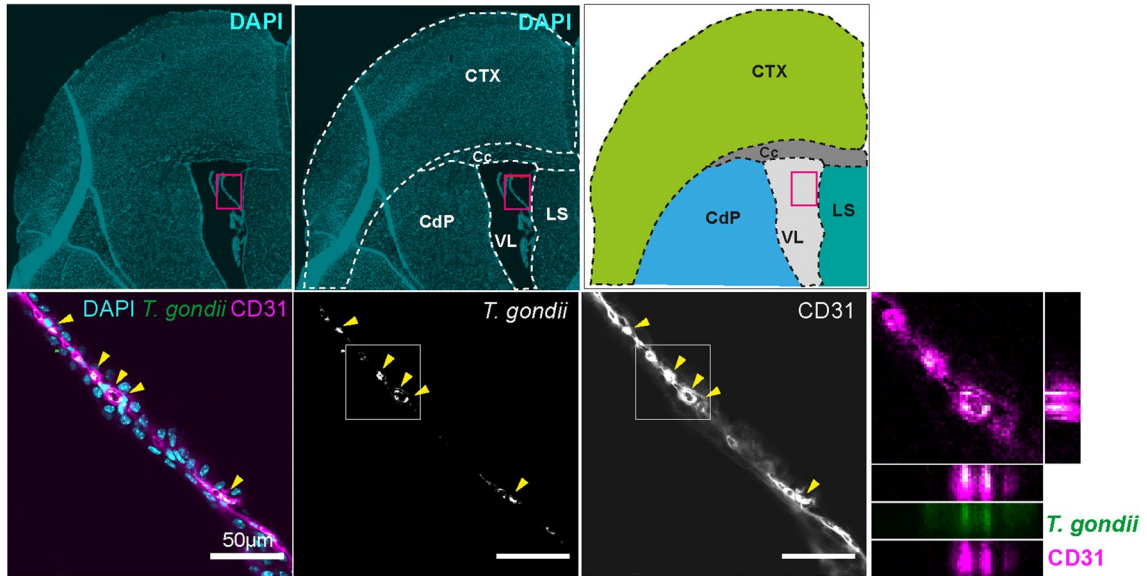
in more details, we first compared the MHCII expression on endothelial cells from CP and remaining brain tissue (Fig. 3A–H). In agreement with the spatiotemporal differences in pathogen distribution (Fig. 1), MHCII upregulation on endothelial cells was first evidenced in the CP followed by later activation of brain endothelial cells (Fig. 3A–H). The definition of endothelial cells as CD45⁻CD31⁺ was sufficient to identify endothelial cells from both tissues, and nor the additional endothelial marker VE-cadherin neither the fibroblastic marker GP38 (podoplanin) improved the recognition of endothelial cells [see Additional file 5]. The kinetics of MHCII expression by microglia was comparable to brain endothelial cells and reached maximum levels at 7 dpi [see Additional file 6]. Moreover, MHCII expression was analyzed on CP epithelial cells even though less than 10% of the cells express this marker, a significant increase was observed [see Additional file 6]. Of note, total mRNA expression of MHCII (*H2-Aa*) in the CP was also increased during infection [see Additional file 7]. Taken together, choroidal endothelial cells responded earlier to *T. gondii* than brain endothelial cells and microglia, indicating that the CP is a critical interface for early parasite recognition.

To further compare the local inflammatory response in the BCSFB versus the BBB, we analyzed the mRNA expression of pro-inflammatory cytokines which play a central role in host defense upon *T. gondii* infection. Therefore, CP and the BMV were isolated from infected brains and expression of IFN- γ , TNF, and IL-6 were measured (Fig. 3I). Compared to the BMV, CP expression of IFN- γ was higher and earlier elevated. BMV only reached comparable IFN- γ levels at 7 dpi. TNF was significantly higher in the CP at both 5 and 7 dpi and IL-6 levels peaked at 3 dpi and was higher in the CP at 7 dpi (Fig. 3I). We also evaluated the expression of type I interferon- β (IFN- β , *Ifnb1*), which were highly expressed in the CP [see Additional file 7]. Furthermore, the cell-autonomous immune response against intracellular *T. gondii* infection is mediated by IFN- γ -inducible GTPases, designated as host-defense factors (*Irgm1*, *Igtp*, *Gbp2b*). Following the elevated IFN- γ levels, we detected higher expression of those genes on the CP compared to the BMV (Fig. 3J). Previous studies have shown specific immune cell

(See figure on next page.)

Fig. 2 *Toxoplasma gondii* infection of endothelial and immune cells in the CP. **A** Animals were infected *i.p.* with 1×10^5 *T. gondii* type II PTG-GFP tachyzoites. The brains were isolated at 7 dpi, and coronal sections were immune-stained with anti-GFP (green), anti-CD31 (magenta) and DAPI (cyan). First row indicate the location of the CP (magenta rectangle) in the lateral ventricle (VL) according to the mouse brain atlas. Second row magnify the CP area above. Yellow arrowheads indicate the detection of parasites co-localized with endothelial cells (CD31). Scale bars = 50 μ m **B** Isolated CPs from animals infected *i.p.* with 1×10^5 PTG-GFP tachyzoites were immune-stained as whole-tissue mount with anti-CD45 (blue), anti-SAG1 (red), and anti-CD31 (green). Animals were infected at the same time, but tissues were analyzed at 3, 5 and 7 dpi. Yellow arrows indicate CD45/SAG1 co-localization, showing immune cells carrying parasites through the BCSFB. Arrowheads indicate co-localization of CD31/SAG1, and asterisks represent SAG1 signal alone. White square indicates magnified area of co-localization signal and orthogonal views of a z-stack analysis. GFP signal plus SAG1 staining were detected in the same channel and colored in red for better visualization. Scale bars = 50 μ m. CTX cortex, Cc corpus callosum, Cdp caudoputamen, LS lateral septal, VL lateral ventricle

A
Brain coronal section - 7dpi



B
Isolated CP

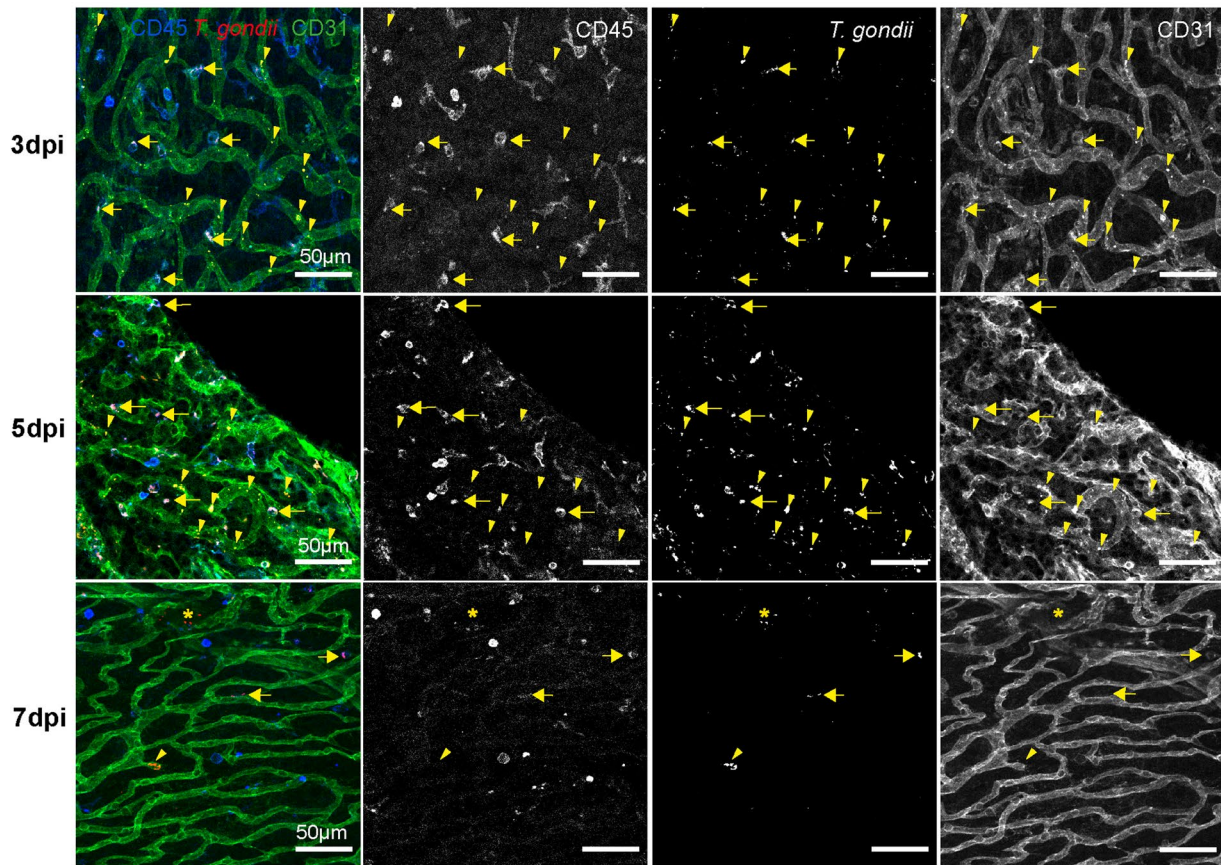
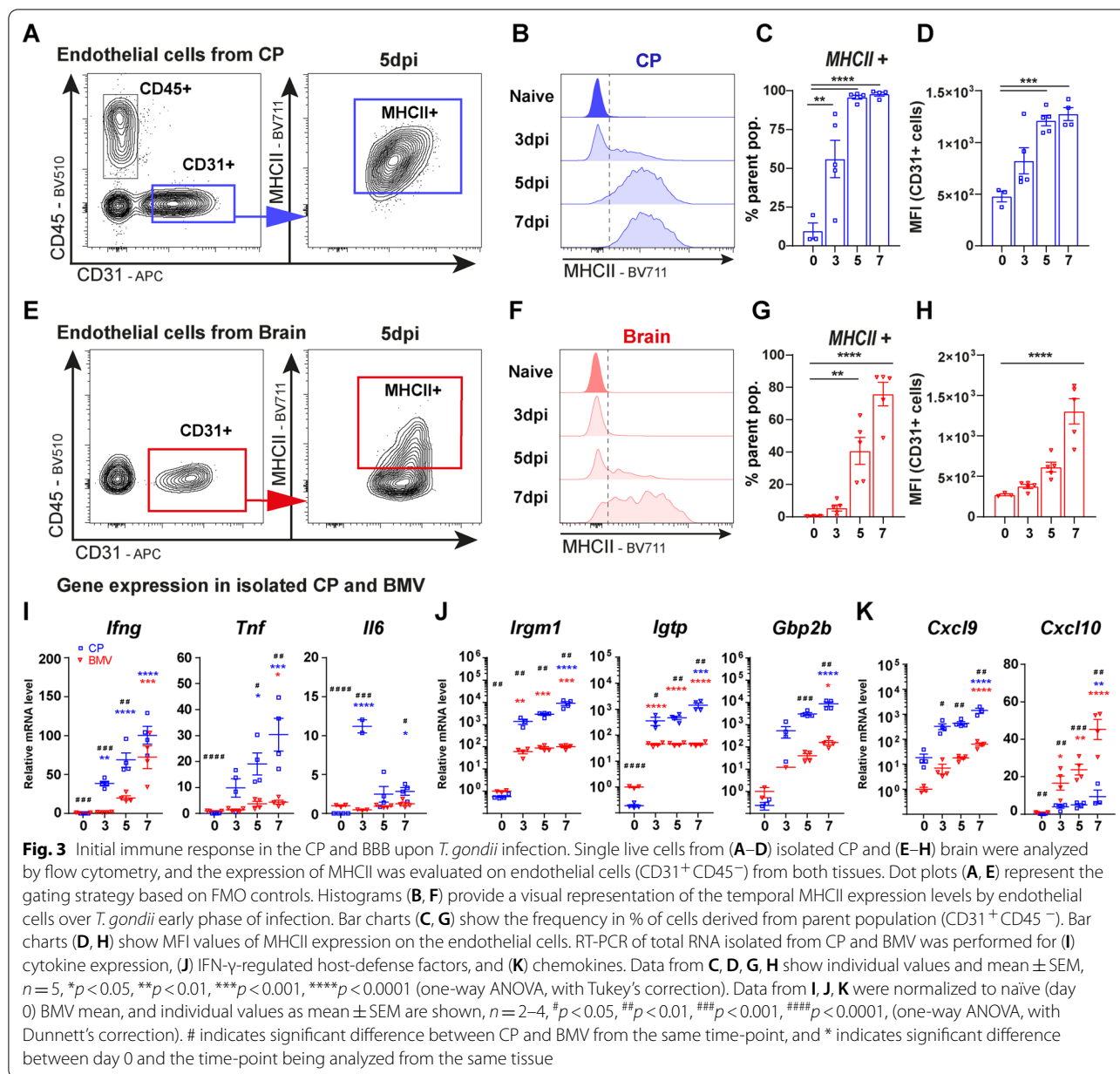


Fig. 2 (See legend on previous page.)



trafficking molecules to be upregulated on CP epithelial cells in the presence of IFN- γ and TNF [50]. Accordingly, CXCL9 expression was higher in CP throughout the observation period. On the contrary, CXCL10 was more pronounced in the BMV, and both chemokines were progressively increased during the infection (Fig. 3K). At last, M-CSF (macrophage colony-stimulating factor, *Csf1*) and CX3CL1 (fractalkine), which are chemokines involved in monocyte trafficking across the BCSFB [52] were also found upregulated in the CP at 7 dpi, while no alteration was detected for M-CSF on BMV [see Additional file 7]. Of note, ICAM-1 involved in the general trafficking of

immune cells was also upregulated at the CP [see Additional file 7]. Overall, *T. gondii* elicited an early and local immune response at the BCSFB, with the expression of pro-inflammatory cytokines, IFN- γ -inducible GTPases, and leukocyte trafficking molecules.

Loss of TJ integrity affects BCSFB function in early infection

TJ molecules constitute the main components of the paracellular barrier established by CP epithelial cells, therefore they assume an essential role determining cellular and molecular compounds delivered from blood into CNS [25]. To investigate the outcome of *T. gondii*

infection at the BCSFB, we analyzed the expression of TJs in isolated CP tissue over the course of infection. Claudins form the majority group of the integral membrane TJ proteins, which establish complex interactions with intracellular linker proteins like zonula occludens proteins (ZO, *Tjp*) [53]. Upon *T. gondii* infection at the CP, we detected lower expression levels of Claudin-2, -3, -5, and -11 compared to naïve group, suggesting a TJ alteration (Fig. 4A). Moreover, the breakdown of epithelial barriers has been associated with increased activity of matrix metalloproteinases (MMPs), which were indicated to be detrimental for BCSFB integrity during neuroinflammation [33]. Here, infected CP tissue displayed a robust upregulation of MMP-8 and MMP-13 (Fig. 4B), pointing towards a potential involvement of those endopeptidases in the epithelial barrier perturbation upon parasite invasion of the BCSFB. Taken together, the expression levels of claudins and MMPs in the infected CP suggested a barrier disruption. Indeed, immunostaining for Claudin-2 on brain sections showed ruffled-shape irregularities on the contour of CP epithelial cells in infected mice, instead of the smooth and continuous staining pattern depicted in naïve CP (Fig. 4C) [see Additional file 8]. In addition, ZO-1 staining indicates a grade of erasure in the infected CP, interestingly depicted in the same area of Claudin-2 morphological alteration. Finally, we determined whether altered TJ and MMP expression patterns affected CP barrier function. For this purpose, a FITC-dextran permeability assay was performed to assess barrier function in vivo. The extravasation of the fluorochrome-conjugated polysaccharide was quantified in the CSF for CP integrity, and in the remaining brain homogenate for BBB integrity (Fig. 4D). In contrast to the BBB, BCSFB permeability increased over time. A significant difference between both compartments was first visible at 7 dpi and further increased from 10 to 23 dpi. BBB vascular alterations were not depicted [see Additional file 9]. Thus, our results reveal a continuous increase in BCSFB permeability, suggesting long-standing detrimental effects of *T. gondii* infection on CP barrier integrity. Altogether, *T. gondii* infection results in TJs disturbances in the CP, with possible involvement of MMP-8 and MMP-13, culminating in functional loss and increased permeability of the BCSFB.

Response of choroid plexus epithelial cells to *T. gondii* in vitro

For a more detailed characterization of *T. gondii* infection effects in the CP epithelium, we developed an in vitro culture model for murine primary CP epithelial cells. First, we confirmed the ability of the cultivated cells to establish adhesion junctions and express ZO-1 (honeycomb shape) (Fig. 5A). In addition, cell cultures were largely devoid of IBA-1⁺ myeloid cells and contained mainly CD45⁻ CD31⁻ E-cadherin⁺ epithelial cells (Fig. 5B). Subsequently, CP epithelial cells were cultured in the presence or absence of GFP⁺ *T. gondii* and the expression of the TJ proteins ZO-1 and Claudin-2 were quantified (Fig. 6). ZO-1 (Fig. 6A) and Claudin-2 (Fig. 6B) showed a poor and non-continuous distribution, characterized by strand breaks and puncta upon infection, compared to naïve controls. Additionally, the gene expression analysis of the cultivated epithelial cells showed no expression of IFN- γ , but increased expression of IFN- γ -receptor (*Ifngr2*) upon infection. The tissue damage-associated cytokines TNF and IL-6 were also upregulated, and the chemokine CCL2, responsible for myeloid cell recruitment was about 60-fold higher on infected cultures (Fig. 6C). We also detected a discrete reduction of ZO-1 (encoded by *Tjp1*) expression upon infection, without change and in the levels of Claudin-2 and Claudin-11 (Fig. 6D). In agreement with (Fig. 4B), MMP-8 and MMP-13 showed a robust upregulation upon infection, suggesting that CP epithelial cells are relevant source of MMPs (Fig. 6E). Overall, these results demonstrate that epithelial cells from CP directly respond to *T. gondii* infection, and contribute to the local inflammatory response and BCSFB damage.

Discussion

The pivotal role of the CP in the orchestration of neuroinflammation became evident in the recent years [49, 54–56], and distinct pathogens have been described exploiting the CP as gateway into CNS [35]. These microbes cross CNS barriers via paracellular entry, transcellular penetration, or via infected immune cells (“Trojan horse”) [57]. The same mechanisms have been proposed for *T. gondii* invasion of the BBB [23], but only

(See figure on next page.)

Fig. 4 Dysregulated tight junctions in the CP affect BCSFB function during early infection. **A** Tight junctions and **B** MMP-8, and MMP-13 expression analysis (RT-PCR) of total RNA isolated from CP at 3, 5 and 7 dpi. Data show individual values and mean \pm SEM, $n = 2-5$, * $p < 0.05$, ** $p < 0.01$, *** $p < 0.001$, **** $p < 0.0001$ (one-way ANOVA, with Dunnett's correction). **C** Immunofluorescence of coronal brain sections stained for identification of Claudin-2 (green) and ZO-1 (red) tight junctions from naïve and 7 dpi mice. White squares identify the regions of interest shown in higher magnification in the white upper squares. Lower panels indicate the respective inverted separated channels for each staining without DAPI to visualize the protein disturbances. Scale bars = 50 μ m. **D** Functional FITC-dextran permeability assay comparing the leakage of the BCSFB (blue) versus BBB (red) throughout the course of infection. Data show mean \pm SEM ($n = 5$) for each time-point analyzed. **** $p < 0.0001$, # $p < 0.05$, ### $p < 0.0001$. # indicates significant difference between BCSFB and BBB from the same time-point (multiple t -test), and * indicates significant differences between day 0 and the time-point being analyzed from the same barrier type (one-way ANOVA, with Dunnett's correction)

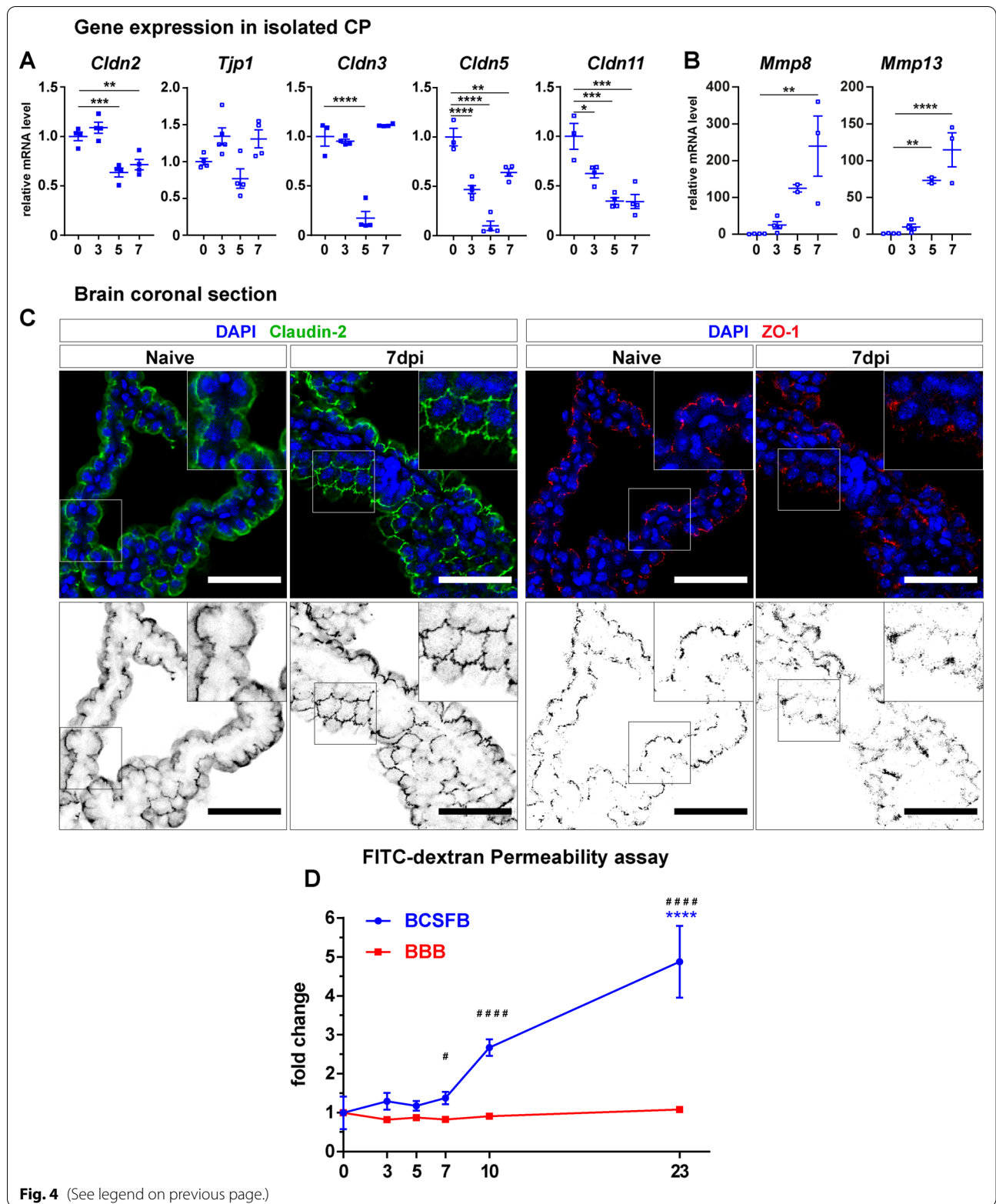
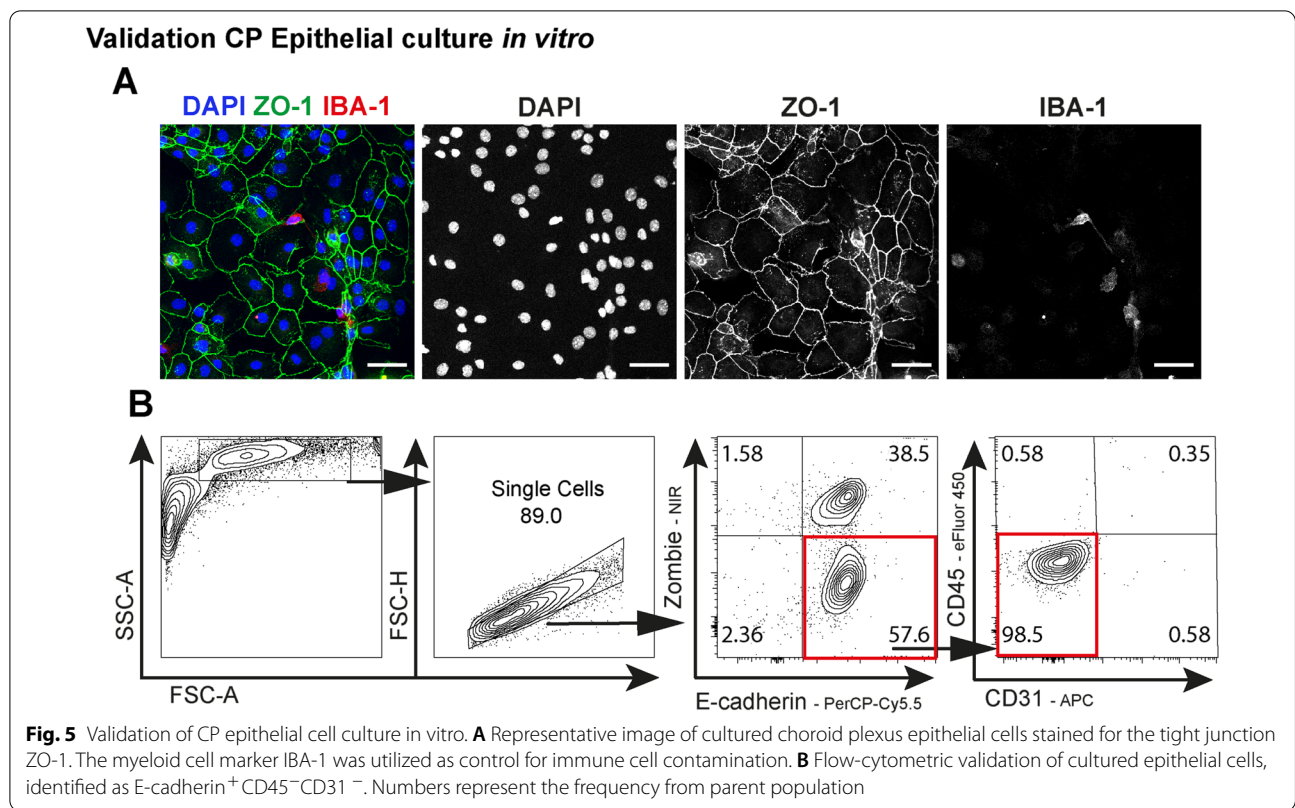


Fig. 4 (See legend on previous page.)



(See figure on next page.)

Fig. 6 Epithelial CP cells response against *T. gondii* *in vitro*. **A, B** Primary cultures of CP epithelial cells were infected for 6 h with reporter *T. gondii* type II PRU-GFP tachyzoites at MOI = 5, and controls remained non-infected. Cultivated cells were immune-stained for detection of **(A)** ZO-1 (red) and **(B)** Claudin-2 (red). DAPI stained the nucleus (blue). GFP-reporter *T. gondii* (green). Scale bars = 50 μm. **C–E** Naïve and infected cultures were analyzed for gene expression of **(C)** cytokines and *Ifngr2*, **(D)** ZO-1 (*Tjp1*) and tight junctions, and **(E)** MMPs. Bar charts show individual mean values of triplicates from a representative experiment, and the mean + SEM ($n = 3$) for each time-point analyzed. Data were normalized by naïve means, besides *Mmp13* which was not detectable on naïve samples * $p < 0.05$, ** $p < 0.01$ (Student's *t*-test)

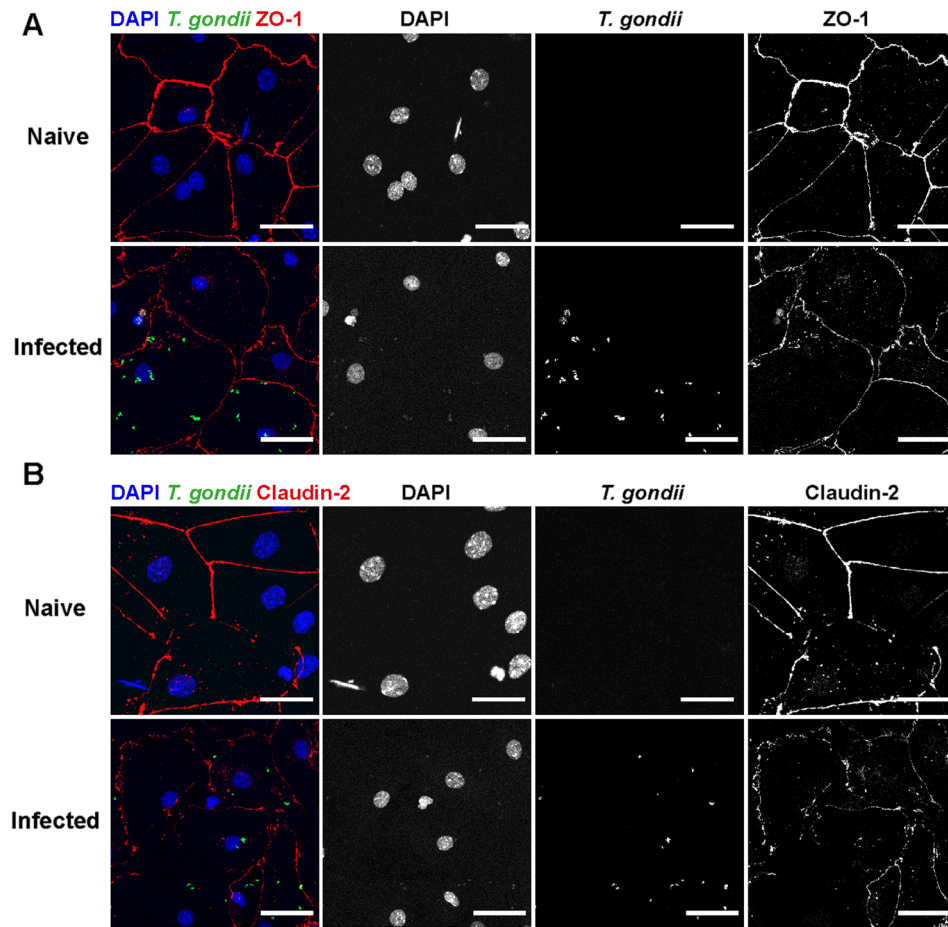
few studies have explored the CP as a gateway for *T. gondii* [36].

Here we demonstrate that *T. gondii* was found in the CP at the onset of infection. In a model of reactivated TE, there was no evidence for the involvement of the CP in *T. gondii* dissemination [37, 38]. Whether parasites are able to translocate from blood to the CSF, via CP, and further infect CSF-inundated areas (e.g., brain, spinal cord) is still not fully understood. In fact, we have previously described the extent of spinal cord pathology in a model of experimental chronic toxoplasmosis, suggesting that parasites translocate into CSF while the infection progresses [58]. Currently, the lack of tools to specifically block parasite entry into one or another barrier presents a major challenge to unveil their respective contributions to the parasite invasion. Here, we propose that CP infection is the initial step to the development of the neuroinflammation, resulting in the disruption of the BCSFB.

Evidences show that the collapse of this barrier and its regulatory mechanisms allow immune cells to enter the CNS and initiate neuroinflammatory diseases [27]. As the disease evolves, the parasite spread increases, e.g., through circulation of infected monocytes which simultaneously can cross the CNS via transposition of BBB and CP. It is likely that the higher parasite burden on BMV at 7 dpi indicate parasite shuttling to small CNS capillaries due to infected embolized monocytes, as suggested by previous studies [59].

Our findings suggest that the activation of the CP vasculature is involved in the orchestration of the anti-parasitic immune responses at early time points of infection. We observed that choroidal endothelial cells upregulated MHCII expression in response to *T. gondii* earlier than brain endothelial cells or microglia. Of note, brain endothelial cells have been described to serve as a replicative niche for *T. gondii* invasion of the CNS [7], but

T. gondii* infection of CP Epithelial culture *in vitro



Gene expression in infected Epithelial cells *in vitro*

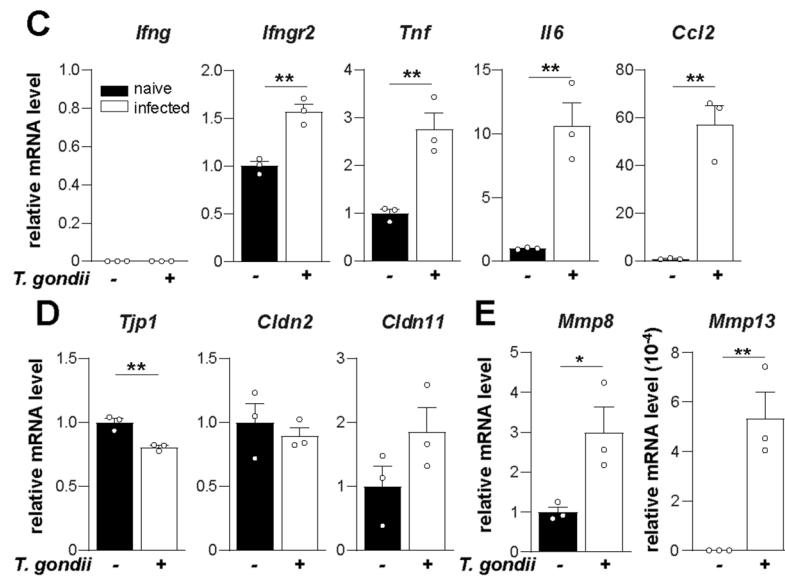


Fig. 6 (See legend on previous page.)

whether activated endothelial cells can control parasite replication in vivo is still unknown. Though, early MHCII presentation by CP endothelial cells suggests that they may play a role in antigen-presentation and interaction with T cells during *T. gondii* infection. They likely initiate a prompt recruitment of immune cells to the CP, orchestrating the onset of infection-induced neuroinflammation. In line with our findings, CP has been considered previously as a niche for T-cell proliferation and stimulation within the CNS [60]. Vascular and epithelial alterations at the CP, followed by other alterations like reduced choroidal synthesis, transport capacity, and CSF secretion were shown during aging, and were described to be intensified in Alzheimer's disease [61]. Therefore, our data confirm the CP as an important interface to early pathogen interaction with endothelial cells, likely promoting damage recognition, antigen-presentation and immune cell recruitment.

Infections at the BCSFB has proven to promote CNS inflammation, inducing cytokines and chemokine secretion locally, and in the CSF, mediating immune cell activation and recruitment [62]. The CP senses CNS injury and rapidly responds to inflammation, upregulating the expression of adhesion molecules and chemokines receptors essential for leukocyte trafficking [50]. Upon the establishment of infection at the CP, we have found that *T. gondii* elicited early and local immune response at the BCSFB, with expression of pro-inflammatory cytokines, IFN- γ -inducible GTPases, and leukocyte trafficking molecules. In face of early detection of CD45⁺ cells associated to *T. gondii* on the CP, we hypothesize that a transient burden of extracellular parasites in the blood likely reach the CP interface, infecting the choroidal endothelial cells and challenging the resident stromal macrophages and epithelial cells. Additionally, IFN- γ , TNF and IL-6 upregulation in the CP of infected mice might be due to the combined action of immune and epithelial cells, which showed elevated levels of gene expression after in vitro culture with *T. gondii*. This suggests a direct anti-parasitic, pro-inflammatory response of the CP epithelial cells. However, IFN- γ gene expression was only detectable in the CP in vivo, but not in CP epithelial cells co-cultured with *T. gondii*. This indicates that IFN- γ expression is restricted to immune cells. Whether they are CP-resident and/or recruited immune cells from the periphery remains to be clarified. IFN- γ -signaling through CP epithelium have been shown to tightly regulate cell recruitment into CNS [50], and probably will determine the immune cell dynamics through the CP upon *T. gondii* infection. Besides, we detected upregulation of IFN- γ -receptor (*Ifngr2*) on in vitro-infected

CP epithelial cells, likely resulting in the increased expression of leukocyte trafficking genes CSF-1, CX3CL1, ICAM-1, CXCL9 and CXCL10, as previously described [50]. Moreover, we found CXCL9 more expressed in CP rather than in BMV through the first week of infection. Indeed, CXCL9 is known to induce T-cell activation and recruitment into the brain during cerebral toxoplasmosis [63]. Hereby, CXCL9 could be a differential trafficking molecule expressed by the CP to specifically modulated the control of *T. gondii* infection.

Dysfunctional BCSFB is part of the pathophysiology leading to increased neuroinflammation [32]. At the BCSFB, the permeability is determined by TJ, specifically the Claudin-family proteins. Claudin-1, -2, -3 are highly expressed in the CP, and have been shown to be sensitive to inflammation [64–67]. In our analysis, Claudin-2 was downregulated and structurally disorganized within CP epithelial cells, displaying a ruffled shape upon infection. TJ ruffling frequently correlates with increased paracellular permeability caused by altered anchoring into actin filaments [68–70]. This anchoring is dependent on the scaffold protein ZO-1, which here displayed a grade of erasure in the infected CP. Accordingly, alterations of Claudins and ZO-1 in the CP have also been described in experimental autoimmune encephalomyelitis (EAE) and LPS-sepsis models [71, 72]. Of note, the infection of BCSFB by *Trypanosoma brucei* has indicated direct parasite interactions with Claudins of the CP, although the mechanisms of how they induce TJs opening is still not known [73, 74]. Still, the disruption of the TJ has been associated to the activity of MMPs enzymes implicated on BCSFB breakdown in neurodegenerative diseases and bacterial meningitis [29, 75]. We detected increased expression levels of the MMP-8 and MMP-13 on the infected CP, with both upregulated on in vitro CP epithelial cultures after *T. gondii* infection. Indeed, previous studies have described MMP-8 contribution to BCSFB leakage, and MMP-13 association with TJ dysregulation [31, 76].

Importantly, here we discovered that the CP damage extended to the chronic phase of experimental murine toxoplasmosis, presented by increased BCSFB permeability, which correlates to our previous findings on neuronal impairment during chronic toxoplasmosis [18, 20, 39, 77]. Therefore, we propose that the substantial change on the CP permeability has detrimental implications for CSF composition and impairment of the CNS drainage. Both aspects may contribute to the increased neuroinflammation and subsequent neuronal damage during toxoplasmosis.

Conclusion

In summary, we detected that the CP is initially infected early after the onset of *T. gondii* infection, where next to CP endothelial cells also immune cells are targeted, determining a rapid inflammatory response and loss of BCSEB integrity and functionality. These processes are likely driven by TJ disturbance of Claudins within CP epithelial cells and by MMP activity. Thus, dysfunctional BCSEB may early enhance and further contribute to *T. gondii*-induced neuroinflammation, therefore emerging as a crucial target for new therapeutic approaches in cerebral toxoplasmosis.

Abbreviations

AF488: Alexa Fluor 488; AF555: Alexa Fluor 555; AF594: Alexa Fluor 594; AF647: Alexa Fluor 647; ANOVA: Analysis of variance; BBB: Blood–brain barrier; BCSEB: Blood–cerebrospinal fluid barrier; BMV: Brain microvessels; CCL2: Chemokine (C–C motif) ligand 2; CD: Cluster of differentiation; CNS: Central nervous system; CP: Choroid plexus; CP-BAMS: Choroid plexus border-associated macrophages; CSF: Cerebrospinal fluid; CX3CL1: Chemokine (C-X3-C motif) ligand 1; CXCL10: Chemokine (C-X-C motif) ligand 10; CXCL9: Chemokine (C-X-C motif) ligand 9; DAAD: Deutscher Akademischer Austauschdienst; DAPI: 4',6-Diamidino-2-phenylindole; DFG: Deutsche Forschungsgemeinschaft; DMEM: Dulbecco's modified Eagle medium; DNA: Deoxyribonucleic acid; DNase I: Deoxyribonuclease type I; dpi: Days post-infection; EDTA: Ethylenediamine tetraacetic acid; EGF: Epidermal growth factor; FACS: Fluorescence-activated cell sorting; FBS: Fetal bovine serum; FITC: Fluorescein isothiocyanate; Gbp2b: Guanylate binding protein 1; GFP: Green fluorescent protein; HBSS: Hank's balanced salt solution; HEPES: 4-(2-Hydroxyethyl)-1-piperazine ethanesulfonic acid; HFF: Human foreskin fibroblasts; IBA-1: Ionized calcium binding adaptor molecule 1; ICAM-1: Intercellular adhesion molecule 1; Ifng2: IFN- γ -receptor; IFN- β : Type I interferon-beta; IFN- γ : Interferon gamma; IgG: Immunoglobulin G; Igtg: Interferon gamma-induced GTPase; IL-6: Interleukin 6; Irgm1: Immunity-related GTPase family M protein 1; ITS: Insulin–transferrin–selenite; LPS: Lipopolysaccharides; M-CSF: Macrophage colony-stimulating factor; MHCII: Major histocompatibility complex type II; MMPs: Metalloproteinases; MOI: Multiplicity of infection; NEEA: Non-essential amino acids; NGS: Normal goat serum; OCT: Optimal cutting temperature; PBS: Phosphate-buffered saline; PCR: Polymerase chain reaction; PDGFR β : Platelet derived growth factor receptor β ; PFA: Paraformaldehyde; PLL: Poly-L-lysine; RNA: Ribonucleic acid; RT: Room temperature; RT-qPCR: Quantitative reverse transcription PCR; SAG1: Surface antigen 1; SEM: Standard error of the mean; *T. gondii*: *Toxoplasma gondii*; TE: Toxoplasma encephalitis; Tjp1: Tight junction protein-1; TJs: Tight junctions; TNF: Tumor necrosis factor; TTR: Transthyretin; ZO-1: Zona occludens-1.

Supplementary Information

The online version contains supplementary material available at <https://doi.org/10.1186/s12974-021-02370-1>.

Additional file 1: Table S1. Oligonucleotide primers used for qPCR and RT-qPCR.

Additional file 2. Detection of *T. gondii* on BMV, brain with removed CP and Spinal cord. Animals were infected *i.p.* with 2 cysts of *T. gondii* type II ME49. CPs were removed and the remaining brain tissue was processed for isolation of BMVs. (A) BMVs from 7 dpi were stained to identify pericytes (PDGFR β), *T. gondii* (SAG1), and the tight junction ZO-1. White square area is shown in higher magnification on the right image, and the yellow arrow points to the disseminated signal for *T. gondii*. (B) Parasite burden in spleens of infected mice at 3, 5 and 7 dpi. The analysis was performed based on the presence of B1 gene of *T. gondii* (TgB1) normalized to the murine gene *Asl*. Data were normalized to the mean values of 3 dpi, and bar charts show individual values of a representative experiment, and

mean \pm SEM, $n = 4$, * $p < 0.05$ (multiple t-test, with Holm-Sidak correction). (C) Brains were isolated, CP removed, and remaining total brain homogenate was processed for parasite detection. (D) Spinal cords from infected mice were also used to quantify parasite burden. The analysis was performed based on expression of *Sag1* gene normalized to *Hprt* expression. Bar charts show individual values of a representative experiment, and mean \pm SEM, $n = 4$ (multiple t-test, with Holm-Sidak correction).

Additional file 3. Detection of *T. gondii* in the CP and brain. Animals were infected *i.p.* with 2 cysts of *T. gondii* type II ME49. The brains were isolated, and coronal sections or CP whole mount were immune-stained with anti-SAG1 (light blue), anti-CD31 (red), anti-Ecadherin (green) and DAPI (dark blue). (A) Confocal image of parasite detection on endothelial cells at 7 dpi. (B) Magnified region of interested previously identified by white square. (C) Parasites identified in the brain cortex, and white square region is magnified in (D). (E) Parasites on CP and adjacent brain ventricular areas at 7 dpi. (F) CP whole tissue mount from animals infected *i.p.* with 1×10^5 *T. gondii* type II PRU-tdTomato tachyzoites, showing detection of parasites inside immune and endothelial cells at 3 dpi.

Additional file 4. IBA-1 staining and morphological identification of CP resident macrophages. Brain coronal sections of naive animals were stained for identification of CP resident macrophages (elongated cells, red) indicated by yellow arrow. White squares indicate magnified region of interested. Scale bars = 50 μ m.

Additional file 5. Alternative surface marker for identification of endothelial cells. Single cells suspensions obtained from CP (A–D), brain (E–H), liver (I–K) and lymph nodes (L–M) were digested and processed under the same conditions, and additional surface markers gp38 and VE-cadherin were used to verify identification of endothelial cells. Dot plots and numbers are from a representative sample. Bar charts represent the frequency in % of cells from parent population. Data represent individual values and mean \pm SEM, $n = 3$.

Additional file 6. MHCII expression by microglia and CP epithelial cells. Single cells suspensions were discriminated based on FSC-SSC parameters, singlets, and viable cells (Zombie NIR negative). (A) Brain cells were gated and identified as microglia (CD11b $^+$ CD45 int), CD45 $^+$ immune cells, and double negative (DN) cells. (B) Choroid plexus cells were first divided in two main populations based on FSC-SSC. Bigger, viable cells were first defined as CD45 $^-$ CD31 $^-$ then positive for the CP epithelial cell marker TTR (transthyretin). Smaller, viable cells were gated as CD45 $^+$ CD31 $^-$ immune cells, and CD45 $^-$ CD31 $^+$ endothelial cells. (C) Representative contour plots showing microglia and (D) CP epithelial cells MHCII expression at 7 dpi. Bar charts represent the frequency in % of cells from parent population, and MFI values of MHCII expression levels. Data represent individual values and mean \pm SEM, $n = 5$, ** $p < 0.01$, *** $p < 0.001$, **** $p < 0.0001$ (one-way ANOVA, with Tukey's correction).

Additional file 7. Complementary gene expression analysis of CP and BMVs. RT-PCR of total RNA from isolated tissue, for (A) MHCII expression on CP, (B, C) expression of interferon-beta-1 (*ifnb1*) and macrophage colony-stimulating factor (*Csf1*), respectively, in isolated CP and BMV. (D, E) Expression of fractalkine (*Cx3cl1*) and intercellular-adhesion-molecule-1 (*Icam1*) on CP. Data show individual values and mean \pm SEM, $n = 3$ –5, * $p < 0.05$, ** $p < 0.01$, *** $p < 0.001$, **** $p < 0.0001$ (A, D, E, one-way ANOVA with Tukey's correction; B, C, one-way ANOVA with Dunnett's correction).

Additional file 8. Complementary staining of Claudin-2 in the CP. Brain coronal sections of naive and 7 dpi animals were stained for identification of morphological alterations of Claudin-2 (green) in CP epithelium. Scale bars = 50 μ m.

Additional file 9. Complementary BBB evaluation of VE-cadherin and ZO-1 upon infection. Animals were infected *i.p.* with 1×10^5 *T. gondii* type II PGT-GFP tachyzoites (green). The brains were isolated at 7 dpi, and coronal sections were immune-stained for identification of VE-cadherin and ZO-1 tight junctions (red). Cortical and hippocampal areas were imaged. White squares identify the regions of interest shown in higher magnification.

Acknowledgements

We thank Petra Grüneberg and Dr. Abidat Schneider for the excellent technical assistance, and all lab colleagues indirectly involved on the execution of this work.

Authors' contributions

CAF and SA performed experiments and analyzed data. JS, LM, AK, OL, MAD, TD critically discussed experimental design, provided material and co-edited the manuscript. CAF and IRD conceived experimental design, and wrote the manuscript. All authors read and approved the final manuscript.

Funding

This work was supported by DFG SFB 854 and SPP1937 to IRD, by the DAAD research grant for doctoral programmes in Germany (n°57214224) and by the Promotionsstipendium of the Medizinischen Fakultät Magdeburg to CAF.

Availability of data and materials

The datasets used and/or analyzed during the current study are available from the corresponding author on reasonable request.

Declarations

Ethics approval and consent to participate

All animal experiments were approved by the respective authorities (Landesverwaltungsamt Halle, Sachsen-Anhalt, Germany) in accordance with German and European legislation.

Consent for publication

Not applicable.

Competing interests

The authors declare no competing interests.

Author details

¹Institute of Inflammation and Neurodegeneration, Medical Faculty, Otto-Von-Guericke University Magdeburg, Magdeburg, Germany. ²Institute for Microbiology and Hygiene, Charité Medical School, Berlin, Germany. ³Institute of Biophysics, Biological Research Centre, 6726 Szeged, Hungary. ⁴Institute for Medical Microbiology and Hospital Hygiene, Medical Faculty, Otto-Von-Guericke University Magdeburg, Magdeburg, Germany. ⁵Institute of Molecular and Clinical Immunology, Medical Faculty, Otto-Von-Guericke University Magdeburg, Magdeburg, Germany. ⁶Center for Behavioral Brain Sciences, CBBS, Magdeburg, Germany.

Received: 16 September 2021 Accepted: 22 December 2021

Published online: 13 January 2022

References

- Tenter AM, Heckerth AR, Weiss LM. *Toxoplasma gondii*: from animals to humans. *Int J Parasitol*. 2000;30(12–13):1217–58.
- Montoya JG, Liesenfeld O. Toxoplasmosis. *Lancet*. 2004;363(9425):1965–76.
- Wilking H, Thamm M, Stark K, Aebischer T, Seeber F. Prevalence, incidence estimations, and risk factors of *Toxoplasma gondii* infection in Germany: a representative, cross-sectional, serological study. *Sci Rep*. 2016;6:22551.
- Harker KS, Ueno N, Lodoen MB. *Toxoplasma gondii* dissemination: a parasite's journey through the infected host. *Parasite Immunol*. 2015;37(3):141–9.
- Barragan A, Sibley LD. Transepithelial migration of *Toxoplasma gondii* is linked to parasite motility and virulence. *J Exp Med*. 2002;195(12):1625–33.
- Courret N, Darche S, Sonigo P, Milon G, Buzoni-Gatel D, Tardieux I. CD11c and CD11b-expressing mouse leukocytes transport single *Toxoplasma gondii* tachyzoites to the brain. *Blood*. 2006;107(1):309–16.
- Konradt C, Ueno N, Christian DA, Delong JH, Pritchard GH, Herz J, et al. Endothelial cells are a replicative niche for entry of *Toxoplasma gondii* to the central nervous system. *Nat Microbiol*. 2016;1:16001.
- Lachenmaier SM, Deli MA, Meissner M, Liesenfeld O. Intracellular transport of *Toxoplasma gondii* through the blood-brain barrier. *J Neuroimmunol*. 2011;232(1–2):119–30.
- Ueno N, Lodoen MB, Hickey GL, Robey EA, Coombes JL. *Toxoplasma gondii*-infected natural killer cells display a hypermotility phenotype in vivo. *Immunol Cell Biol*. 2015;93(5):508–13.
- Coombes JL, Charsar BA, Han SJ, Halkias J, Chan SW, Koshy AA, et al. Motile invaded neutrophils in the small intestine of *Toxoplasma gondii*-infected mice reveal a potential mechanism for parasite spread. *Proc Natl Acad Sci U S A*. 2013;110(21):E1913–22.
- Bhandage AK, Olivera GC, Kanatani S, Thompson E, Lore K, Varas-Godoy M, et al. A motogenic GABAergic system of mononuclear phagocytes facilitates dissemination of coccidian parasites. *Elife*. 2020;9.
- Olafsson EB, Barragan A. The unicellular eukaryotic parasite *Toxoplasma gondii* hijacks the migration machinery of mononuclear phagocytes to promote its dissemination. *Biol Cell*. 2020.
- Ferguson DJ, Graham DI, Hutchison WM. Pathological changes in the brains of mice infected with *Toxoplasma gondii*: a histological, immunocytochemical and ultrastructural study. *Int J Exp Pathol*. 1991;72(4):463–74.
- Dubey JP, Lindsay DS, Speer CA. Structures of *Toxoplasma gondii* tachyzoites, bradyzoites, and sporozoites and biology and development of tissue cysts. *Clin Microbiol Rev*. 1998;11(2):267–99.
- Dubey JP. History of the discovery of the life cycle of *Toxoplasma gondii*. *Int J Parasitol*. 2009;39(8):877–82.
- Parlog A, Harsan LA, Zagrebelsky M, Weller M, von Elverfeldt D, Mawrin C, et al. Chronic murine toxoplasmosis is defined by subtle changes in neuronal connectivity. *Dis Model Mech*. 2014;7(4):459–69.
- Blanchard N, Dunay IR, Schluter D. Persistence of *Toxoplasma gondii* in the central nervous system: a fine-tuned balance between the parasite, the brain and the immune system. *Parasite Immunol*. 2015;37(3):150–8.
- Lang D, Schott BH, van Ham M, Morton L, Kulikovskaja L, Herrera-Molina R, et al. Chronic toxoplasma infection is associated with distinct alterations in the synaptic protein composition. *J Neuroinflammation*. 2018;15(1):216.
- Burgdorf KS, Trabjerg BB, Pedersen MG, Nissen J, Banasik K, Pedersen OB, et al. Large-scale study of toxoplasma and cytomegalovirus shows an association between infection and serious psychiatric disorders. *Brain Behav Immun*. 2019;79:152–8.
- Parlog A, Schluter D, Dunay IR. *Toxoplasma gondii*-induced neuronal alterations. *Parasite Immunol*. 2015;37(3):159–70.
- Munoz M, Liesenfeld O, Heimesaat MM. Immunology of *Toxoplasma gondii*. *Immunol Rev*. 2011;240(1):269–85.
- Matta SK, Rinkenberger N, Dunay IR, Sibley LD. *Toxoplasma gondii* infection and its implications within the central nervous system. *Nat Rev Microbiol*. 2021.
- Mendez OA, Koshy AA. *Toxoplasma gondii*: entry, association, and physiological influence on the central nervous system. *PLoS Pathog*. 2017;13(7):e1006351.
- Gherzi-Egea JF, Strazielle N, Catala M, Silva-Vargas V, Doetsch F, Engelhardt B. Molecular anatomy and functions of the choroidal blood-cerebrospinal fluid barrier in health and disease. *Acta Neuropathol*. 2018;135(3):337–61.
- Castro Dias M, Mapunda JA, Vladymyrov M, Engelhardt B. Structure and junctional complexes of endothelial, epithelial and glial brain barriers. *Int J Mol Sci*. 2019;20(21).
- Baruch K, Schwartz M. CNS-specific T cells shape brain function via the choroid plexus. *Brain Behav Immun*. 2013;34:11–6.
- Fleischer V, Gonzalez-Escamilla G, Ciolac D, Albrecht P, Kury P, Gruchot J, et al. Translational value of choroid plexus imaging for tracking neuroinflammation in mice and humans. *Proc Natl Acad Sci U S A*. 2021;118(36).
- Engelhardt B, Sorokin L. The blood-brain and the blood-cerebrospinal fluid barriers: function and dysfunction. *Semin Immunopathol*. 2009;31(4):497–511.
- Rosenberg GA. Matrix metalloproteinases and their multiple roles in neurodegenerative diseases. *Lancet Neurol*. 2009;8(2):205–16.
- Vandenbroucke RE. A hidden epithelial barrier in the brain with a central role in regulating brain homeostasis. Implications for aging. *Ann Am Thorac Soc*. 2016;13(Suppl 5):S407–10.
- Vandenbroucke RE, Dejonckheere E, Van Lint P, Demeestere D, Van Wontergem E, Vanlaere I, et al. Matrix metalloprotease 8-dependent extracellular matrix cleavage at the blood-CSF barrier contributes

- to lethality during systemic inflammatory diseases. *J Neurosci*. 2012;32(29):9805–16.
32. Demeestere D, Libert C, Vandenbroucke RE. Therapeutic implications of the choroid plexus-cerebrospinal fluid interface in neuropsychiatric disorders. *Brain Behav Immun*. 2015;50:1–13.
 33. Brkic M, Balusu S, Van Wonterghem E, Gorle N, Benilova I, Kremer A, et al. Amyloid beta oligomers disrupt blood-CSF barrier integrity by activating matrix metalloproteinases. *J Neurosci*. 2015;35(37):12766–78.
 34. Gorle N, Blaecher C, Bauwens E, Vandendriessche C, Balusu S, Vandewalle J, et al. The choroid plexus epithelium as a novel player in the stomach-brain axis during *Helicobacter* infection. *Brain Behav Immun*. 2018;69:35–47.
 35. Lauer AN, Tenenbaum T, Schroten H, Schwerc C. The diverse cellular responses of the choroid plexus during infection of the central nervous system. *Am J Physiol Cell Physiol*. 2018;314(2):C152–65.
 36. Falangola MF, Petito CK. Choroid plexus infection in cerebral toxoplasmosis in AIDS patients. *Neurology*. 1993;43(10):2035–40.
 37. Dellacasa-Lindberg I, Hitziger N, Barragan A. Localized recrudescence of *Toxoplasma* infections in the central nervous system of immunocompromised mice assessed by in vivo bioluminescence imaging. *Microbes Infect*. 2007;9(11):1291–8.
 38. Schluter D, Barragan A. Advances and challenges in understanding cerebral toxoplasmosis. *Front Immunol*. 2019;10:242.
 39. Dusedau HP, Klevevan J, Figueiredo CA, Biswas A, Steffen J, Kliche S, et al. p75(NTR) regulates brain mononuclear cell function and neuronal structure in *Toxoplasma* infection-induced neuroinflammation. *Glia*. 2019;67(1):193–211.
 40. Figueiredo CA, Dusedau HP, Steffen J, Gupta N, Dunay MP, Toth GK, et al. Immunomodulatory effects of the neuropeptide pituitary adenylate cyclase-activating polypeptide in acute toxoplasmosis. *Front Cell Infect Microbiol*. 2019;9:154.
 41. Liu L, Duff K. A technique for serial collection of cerebrospinal fluid from the cisterna magna in mouse. *J Vis Exp*. 2008(21).
 42. Nakagawa S, Deli MA, Kawaguchi H, Shimizudani T, Shimono T, Kittel A, et al. A new blood-brain barrier model using primary rat brain endothelial cells, pericytes and astrocytes. *Neurochem Int*. 2009;54(3–4):253–63.
 43. Menhenniott TR, Charalambous M, Ward A. Derivation of primary choroid plexus epithelial cells from the mouse. *Methods Mol Biol*. 2010;633:207–20.
 44. Lazarevic I, Engelhardt B. Modeling immune functions of the mouse blood-cerebrospinal fluid barrier in vitro: primary rather than immortalized mouse choroid plexus epithelial cells are suited to study immune cell migration across this brain barrier. *Fluids Barriers CNS*. 2016;13:2.
 45. Burg JL, Grover CM, Pouletty P, Boothroyd JC. Direct and sensitive detection of a pathogenic protozoan, *Toxoplasma gondii*, by polymerase chain reaction. *J Clin Microbiol*. 1989;27(8):1787–92.
 46. Lin MH, Chen TC, Kuo TT, Tseng CC, Tseng CP. Real-time PCR for quantitative detection of *Toxoplasma gondii*. *J Clin Microbiol*. 2000;38(11):4121–5.
 47. Butcher BA, Fox BA, Rommereim LM, Kim SG, Maurer KJ, Yarovinsky F, et al. *Toxoplasma gondii* rhoptry kinase ROP16 activates STAT3 and STAT6 resulting in cytokine inhibition and arginase-1-dependent growth control. *PLoS Pathog*. 2011;7(9):e1002236.
 48. Baruch K, Deczkowska A, David E, Castellano JM, Miller O, Kertser A, et al. Aging-induced type I interferon response at the choroid plexus negatively affects brain function. *Science*. 2014;346(6205):89–93.
 49. Baruch K, Ron-Harel N, Gal H, Deczkowska A, Shifrut E, Ndifon W, et al. CNS-specific immunity at the choroid plexus shifts toward destructive Th2 inflammation in brain aging. *Proc Natl Acad Sci U S A*. 2013;110(6):2264–9.
 50. Kunis G, Baruch K, Rosenzweig N, Kertser A, Miller O, Berkutzi T, et al. IFN-gamma-dependent activation of the brain's choroid plexus for CNS immune surveillance and repair. *Brain*. 2013;136(Pt 11):3427–40.
 51. Helms HC, Abbott NJ, Burek M, Cecchetti R, Couraud PO, Deli MA, et al. In vitro models of the blood-brain barrier: an overview of commonly used brain endothelial cell culture models and guidelines for their use. *J Cereb Blood Flow Metab*. 2016;36(5):862–90.
 52. Szymdynger-Chodobska J, Strazielle N, Gandy JR, Keefe TH, Zink BJ, Ghersi-Egea JF, et al. Posttraumatic invasion of monocytes across the blood-cerebrospinal fluid barrier. *J Cereb Blood Flow Metab*. 2012;32(1):93–104.
 53. Solar P, Zamani A, Kubickova L, Dubovy P, Joukal M. Choroid plexus and the blood-cerebrospinal fluid barrier in disease. *Fluids Barriers CNS*. 2020;17(1):35.
 54. Shechter R, Miller O, Yovel G, Rosenzweig N, London A, Ruckh J, et al. Recruitment of beneficial M2 macrophages to injured spinal cord is orchestrated by remote brain choroid plexus. *Immunity*. 2013;38(3):555–69.
 55. Schwartz M, Baruch K. The resolution of neuroinflammation in neurodegeneration: leukocyte recruitment via the choroid plexus. *EMBO J*. 2014;33(1):7–22.
 56. Kunis G, Baruch K, Miller O, Schwartz M. Immunization with a myelin-derived antigen activates the Brain's choroid plexus for recruitment of immunoregulatory cells to the CNS and attenuates disease progression in a mouse model of ALS. *J Neurosci*. 2015;35(16):6381–93.
 57. Dando SJ, Mackay-Sim A, Norton R, Currie BJ, St John JA, Ekberg JA, et al. Pathogens penetrating the central nervous system: infection pathways and the cellular and molecular mechanisms of invasion. *Clin Microbiol Rev*. 2014;27(4):691–726.
 58. Mohle L, Parlog A, Pahnke J, Dunay IR. Spinal cord pathology in chronic experimental *Toxoplasma gondii* infection. *Eur J Microbiol Immunol (Bp)*. 2014;4(1):65–75.
 59. Drewry LL, Jones NG, Wang Q, Onken MD, Miller MJ, Sibley LD. The secreted kinase ROP17 promotes *Toxoplasma gondii* dissemination by hijacking monocyte tissue migration. *Nat Microbiol*. 2019;4(11):1951–63.
 60. Strominger I, Elyahu Y, Berner O, Reckhow J, Mittal K, Nemirovsky A, et al. The choroid plexus functions as a niche for T-cell stimulation within the central nervous system. *Front Immunol*. 2018;9:1066.
 61. Serot JM, Zmudka J, Jouanny P. A possible role for CSF turnover and choroid plexus in the pathogenesis of late onset Alzheimer's disease. *J Alzheimers Dis*. 2012;30(1):17–26.
 62. Meeker RB, Williams K, Killebrew DA, Hudson LC. Cell trafficking through the choroid plexus. *Cell Adh Migr*. 2012;6(5):390–6.
 63. Ochiai E, Sa Q, Brogli M, Kudo T, Wang X, Dubey JP, et al. CXCL9 is important for recruiting immune T cells into the brain and inducing an accumulation of the T cells to the areas of tachyzoite proliferation to prevent reactivation of chronic cerebral infection with *Toxoplasma gondii*. *Am J Pathol*. 2015;185(2):314–24.
 64. Meoli L, Gunzel D. Channel functions of claudins in the organization of biological systems. *Biochim Biophys Acta Biomembr*. 2020;1862(9):183344.
 65. Kratzer I, Vasiljevic A, Rey C, Fevre-Montange M, Saunders N, Strazielle N, et al. Complexity and developmental changes in the expression pattern of claudins at the blood-CSF barrier. *Histochem Cell Biol*. 2012;138(6):861–79.
 66. Bhat AA, Syed N, Therachiyil L, Nisar S, Hashem S, Macha MA, et al. Claudin-1, a double-edged sword in cancer. *Int J Mol Sci*. 2020;21(2):569.
 67. Zhou B, Flodby P, Luo J, Castillo DR, Liu Y, Yu FX, et al. Claudin-18-mediated YAP activity regulates lung stem and progenitor cell homeostasis and tumorigenesis. *J Clin Invest*. 2018;128(3):970–84.
 68. Saeedi BJ, Kao DJ, Kitzenberg DA, Dobrinskikh E, Schwisow KD, Masterson JC, et al. HIF-dependent regulation of claudin-1 is central to intestinal epithelial tight junction integrity. *Mol Biol Cell*. 2015;26(12):2252–62.
 69. Kam KR, Walsh LA, Bock SM, Ollerenshaw JD, Ross RF, Desai TA. The effect of nanotopography on modulating protein adsorption and the fibrotic response. *Tissue Eng Part A*. 2014;20(1–2):130–8.
 70. Samak G, Gangwar R, Crosby LM, Desai LP, Wilhelm K, Waters CM, et al. Cyclic stretch disrupts apical junctional complexes in Caco-2 cell monolayers by a JNK-2-, c-Src-, and MLCK-dependent mechanism. *Am J Physiol Gastrointest Liver Physiol*. 2014;306(11):G947–58.
 71. Shrestha B, Paul D, Pachter JS. Alterations in tight junction protein and IgG permeability accompany leukocyte extravasation across the choroid plexus during neuroinflammation. *J Neuropathol Exp Neurol*. 2014;73(11):1047–61.
 72. Marques F, Sousa JC, Coppola G, Falcao AM, Rodrigues AJ, Geschwind DH, et al. Kinetic profile of the transcriptome changes induced in the choroid plexus by peripheral inflammation. *J Cereb Blood Flow Metab*. 2009;29(5):921–32.
 73. Mogk S, Meiwes A, Bosselmann CM, Wolburg H, Duszzenko M. The lane to the brain: how African trypanosomes invade the CNS. *Trends Parasitol*. 2014;30(10):470–7.

74. Mogk S, Meiwes A, Shtopel S, Schraermeyer U, Lazarus M, Kubata B, et al. Cyclical appearance of African trypanosomes in the cerebrospinal fluid: new insights in how trypanosomes enter the CNS. *PLoS ONE*. 2014;9(3):e91372.
75. Leppert D, Leib SL, Grygar C, Miller KM, Schaad UB, Hollander GA. Matrix metalloproteinase (MMP)-8 and MMP-9 in cerebrospinal fluid during bacterial meningitis: association with blood-brain barrier damage and neurological sequelae. *Clin Infect Dis*. 2000;31(1):80–4.
76. Vandenbroucke RE, Dejonckheere E, Van Hauwermeiren F, Lodens S, De Rycke R, Van Wonterghem E, et al. Matrix metalloproteinase 13 modulates intestinal epithelial barrier integrity in inflammatory diseases by activating TNF. *EMBO Mol Med*. 2013;5(7):1000–16.
77. French T, Dusedau HP, Steffen J, Biswas A, Ahmed N, Hartmann S, et al. Neuronal impairment following chronic *Toxoplasma gondii* infection is aggravated by intestinal nematode challenge in an IFN-gamma-dependent manner. *J Neuroinflammation*. 2019;16(1):159.

Publisher's Note

Springer Nature remains neutral with regard to jurisdictional claims in published maps and institutional affiliations.

Ready to submit your research? Choose BMC and benefit from:

- fast, convenient online submission
- thorough peer review by experienced researchers in your field
- rapid publication on acceptance
- support for research data, including large and complex data types
- gold Open Access which fosters wider collaboration and increased citations
- maximum visibility for your research: over 100M website views per year

At BMC, research is always in progress.

Learn more biomedcentral.com/submissions

